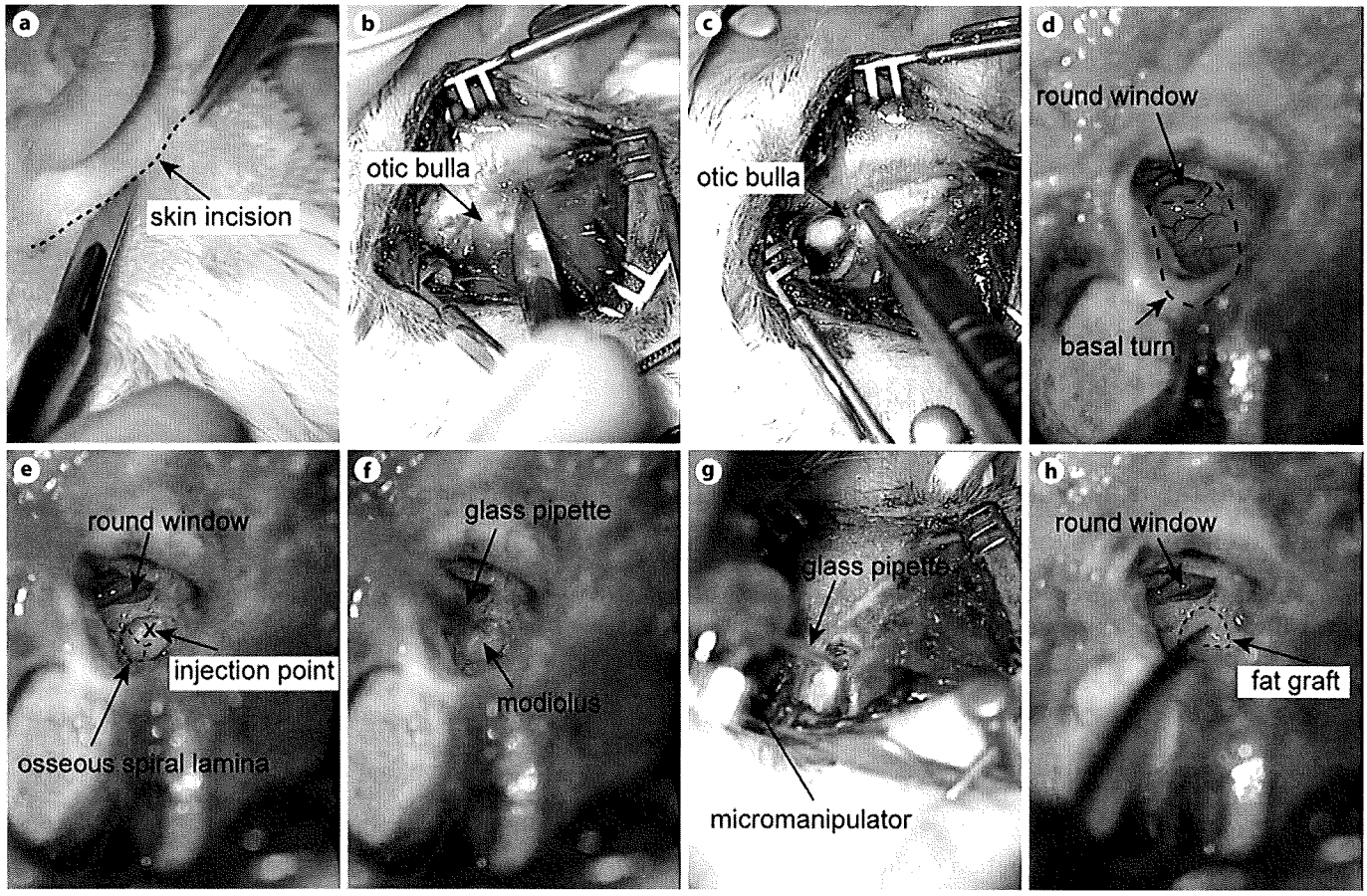

Fig. 1. Surgical procedure for cell transplantation into the cochlear modiolus. **a** Skin incision is made in the retroauricular region. **b** An otic bulla is exposed. **c** A small hole on the bulla is made using a drill. **d** The round window and the basal turn of the cochlea are observed through an opening on the bulla. An interrupted line indicates the location of the basal turn. **e** Cochleostomy is performed on the basal portion of the cochlea corresponding to the location of the scala tympani. A dotted line indicates the location of the osseous spiral lamina. A cross indicates the injection point. **f**, **g** A glass pipette is inserted into the cochlear modiolus using a micromanipulator. **h** The cochleostomy site is closed with a fat graft (dotted line).

evaluated the functional and histological damage to the host SGNs. To evaluate cell transplantation efficiency, we examined the survival of the transplanted ES cell-derived neurons in the cochlear modiolus of guinea pigs. The level of surgical invasiveness was estimated by measuring electrically evoked auditory brainstem responses (eABRs) and SGN densities in Rosenthal's canal following an injection of 5 μl of saline.

Materials and Methods

Animals

A total of 12 Hartley strain guinea pigs weighing 350–400 g were purchased from Japan SLC Inc. (Hamamatsu, Japan). All of the animals had otoscopically normal tympanic membranes and normal hearing, as determined by tone-burst ABR. The Animal Research Committee of the Graduate School of Medicine, Kyoto University, Japan, approved all of the experimental protocols. Animal care was carried out under the supervision of the Institute of Laboratory Animals of the Graduate School of Medicine, Kyoto University. All of the experimental procedures were performed in accordance with the National Institutes of Health Guidelines for the Care and Use of Laboratory Animals.

Surgical Procedure

The animals were anesthetized with an intramuscular injection of ketamine (75 mg/kg) and xylazine (9 mg/kg), and body temperature was maintained at 37 ± 1°C using a heating pad. We used a conventional retroauricular approach in the lateral recumbent position (fig. 1a). After exposure of the otic bulla (fig. 1b), a small hole was made on the otic bulla to expose the round window niche and the basal turn of the cochlea (fig. 1c, d). After fixation of the head position using clay and surgical tape, cochleostomy was performed

on the basal portion of the cochlea to visualize the cochlear modiolus through the scala tympani (fig. 1e). A fine glass pipette was made with a Flaming/Brown micropipette puller (Sutter Instrument Co., Novato, Calif., USA), with the tip cut with a fine blade to make an outer diameter of approximately 100 μm. A micromanipulator was used to insert the glass pipette, which was connected to a microsyringe (Hamilton, Reno, Nev., USA), into the cochlear modiolus of the basal portion of the cochlea (fig. 1f, g). After removal of the perilymph with filter paper, we directly inserted the glass pipette into the bony wall of the cochlear modiolus from a point slightly basal to the junction of the osseous spiral lamina and the modiolus (fig. 1f). In this particular region, a glass pipette is capable of penetrating the bony wall of the cochlear modiolus due to the thickness of the bony wall. Subsequently, we infused 5 μl of the substrate through the glass pipette using a microinfusion pump set at a rate of 1 μl/min. The glass pipette was removed 1 min after stopping the infusion. Finally, the cochleostomy site was closed with a fat graft and then covered with fibrin glue (fig. 1h).

Efficiency of the Cell Transplantation Procedure

We estimated the transplant survival of mouse ES cell-derived neural progenitors in the cochlear modiolus using histological analysis. Mouse G4-2 ES cells (provided by H. Niwa of Riken CDB, Kobe, Japan) that were derived from the E14tg2ab ES cell line and which carried the EGFP gene driven by the CAG promoter were used as the transplant source. Neural induction of ES cells was performed by stromal cell-inducing activity [10] before transplantation. Briefly, undifferentiated ES cells were cultured on a feeder layer of PA6 stromal cells (RCB1127; Riken Cell Bank, Tsukuba, Japan) in Glasgow's modified Eagle's medium (GMEM; Invitrogen, Carlsbad, Calif., USA) supplemented with 5% knockout serum replacement (Invitrogen), 1 mM pyruvate (Sigma, St. Louis, Mo., USA), 0.1 mM nonessential amino acids (Invitrogen), and 0.2 mM 2-mercaptoethanol (Wako, Osaka, Japan). Colonies that formed on the PA6 monolayer after 6 days of culture were isolated and prepared as suspensions of 10^4 cells/μl GMEM.

In 4 guinea pigs, 5 μl of the cell suspensions were injected into the cochlear modiolus in each animal using the procedure described above. At 1 week after cell transplantation, the otic bullae of the experimental animals were opened under ketamine and xylazine anesthesia, and then 4% paraformaldehyde in 0.01 M phosphate-buffered saline at pH 7.4 was perfused into the perilymph from the round window. The animals were deeply anesthetized with a lethal dose of ketamine and xylazine that was perfused intracardially with physiological saline, followed by infusion of the same fixative. The temporal bones were then collected and immersed in the same fixative for 4 h at 4°C. Specimens (10 μm thick) were prepared using a cryostat after decalcification with 0.1 M ethylenediaminetetraacetic acid in phosphate-buffered saline for 3 weeks at 4°C. From each cochlea, three mid-modiolus sections were stained with 2 μg/ml 4′,6-diamino-2-phenylindole dihydrochloride (DAPI; Molecular Probes, Eugene, Oreg., USA), and then viewed with a Nikon Eclipse E600 fluorescence microscope (Nikon, Tokyo, Japan). Settlement of transplants was determined by the existence of both EGFP- and DAPI-positive cells in Rosenthal's canal or the cochlear modiolus.

Functional Estimation of Surgical Invasiveness

We injected 5 μl of physiological saline into the modiolus of the left cochlea of each of 8 guinea pigs. Functional damage was

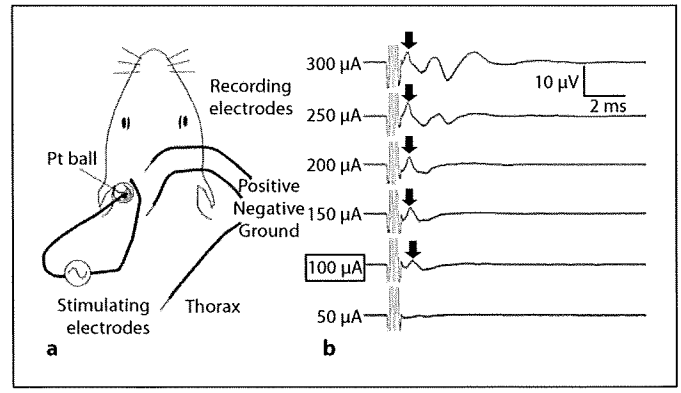

Fig. 2. Measurement of eABRs. **a** A platinum ball electrode is inserted into the scala tympani in the basal portion of the cochlea. Another wire serves as extracochlear ground for monopolar stimulation, and is fixed to the temporal bone. For recording, three electrodes are used (positive; vertex, negative; neck, ground; thorax). **b** The threshold is defined as the smallest current amplitude required to evoke a response within a latency of 4 ms after stimulus onset. Arrows indicate the first positive wave after stimulus onset. The threshold of this sample is 100 μA.

evaluated by determining eABR thresholds immediately before and after surgical treatment, and on days 1 and 14 after surgical treatment. eABR measurements were performed in a sound-attenuated and electrically shielded room. One platinum/iridium ball electrode (Nihon Koden, Tokyo, Japan) was inserted into the scala tympani through the cochleostomy site and was then placed approximately 1.5 mm deep from the cochleostomy site. Another electrode was fixed to the temporal bone where it served as an extracochlear ground for monopolar stimulation (fig. 2a).

Biphasic current pulses were generated under computer control using a real-time processor (Tucker-Davis Technologies, Alachua, Fla., USA). Stimuli were altered in 50-μA steps, with the stimulus current levels calibrated by measuring the voltage with an oscilloscope from 1,000 to 10,000 Ω. The responses against electrical stimuli were recorded separately using stainless steel needle electrodes (fig. 2a, vertex positive, neck negative, thorax ground). The electrical stimulus consisted of charge-balanced biphasic current pulses, which occurred 50 times per second. The scalp-recorded response was amplified by 3×10^3 and band-pass-filtered (200–1,500 Hz). The filter output was fed to an analog-to-digital converter and sampled for 10 ms following stimulus onset. For each recording, 500 responses were averaged and then stored for subsequent analysis. Two sets of recordings were made at each current level, and the current amplitude was reduced to levels below threshold. The thresholds for eABRs were determined as described previously [11–15]. The threshold was defined as the smallest current amplitude that was required to evoke a response with a latency of 4 ms following the stimulus onset for both responses (fig. 2b).

Histological Estimation of Surgical Invasiveness

After saline injection into the cochlear modiolus, the temporal bones were collected on days 1 (n = 4) and 14 (n = 4). Right co-

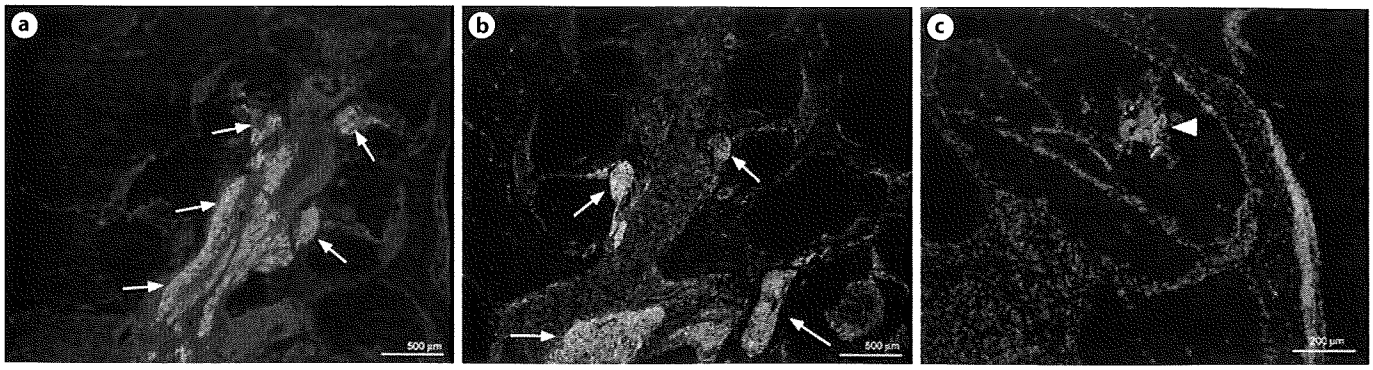

Color version available online

Fig. 3. Locations of transplanted cells in the cochlea. EGFP-expressing cells (green; light gray in the printed version) are found in the cochlear modiolus and Rosenthal's canal from the basal to the middle portion of cochleae (**a**, **b**, arrows). One specimen exhibits settlement of transplanted cells in the scala vestibuli (**c**, arrowhead). Blue fluorescence (rendered dark gray in the printed version) shows nuclear staining with DAPI.

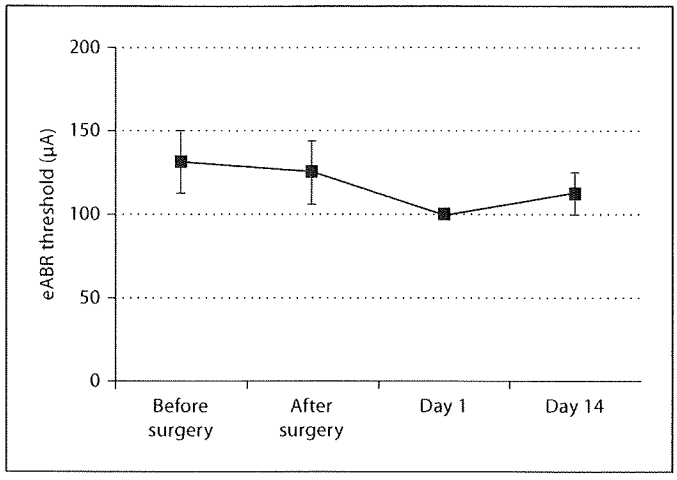

Fig. 4. eABR thresholds immediately before and after surgical treatment, and on days 1 and 14 after surgical treatment. The y-axis shows the mean of eABR thresholds. There are no significant differences in eABR thresholds among experimental groups. Bars represent standard errors.

chleae, which underwent no surgical treatments, were used as controls. After eABR recordings, cochlear specimens were collected and prepared as cryostat sections using a similar procedure as for the transplanted ES cell-derived neurons. Sections were stained with hematoxylin and eosin (HE). SGN counting in Rosenthal's canals was performed in accordance with a method that has previously been described [13–15]. SGN numbers were determined in the basal, mid-basal or second turn from 5 randomly selected mid-modiolar sections of the cochleae that underwent surgery, and from the contralateral cochleae that received no surgical treatment. The cross-sectional areas of Rosenthal's canals were measured using Image/J software (http://www.rsb.info.nist.gov/ij). SGN densities were then calculated by dividing the number of SGNs by the area. This value was used to reduce the variance caused by differences in the cutting directions among the cochlear specimens.

We also evaluated cell infiltration into the cochlea on days 1 and 14 after surgery. The mean numbers of nucleated cells in the scala tympani, scala vestibuli and scala media were determined in the basal, mid-basal and second turns from 5 randomly selected mid-modiolar cochlear sections.

Statistics

The overall effect on the eABR threshold shifts during the surgical procedure was examined by one-way factorial analysis of variance (ANOVA). The values of SGN densities in Rosenthal's canals that were obtained on days 1 or 14 after surgical treatment were compared with those of the contralateral cochleae by an unpaired t test. A p value less than 0.05 was considered statistically significant. All data are presented as the mean ± standard error.

Results

Efficiency of Cell Transplantation

We examined the survival and the location of engrafted ES cell-derived neurons in order to determine the efficiency of cell transplantation with our surgical procedure. All of the cochlear specimens exhibited settlement of the EGFP-expressing cells in Rosenthal's canals or the modioli in the basal portions of the cochleae, indicating that our transplantation procedure using a fine glass pipette was efficient for introducing transplants into the cochlear modiolus. EGFP-positive cells were also identified in the middle portion of the cochlear modiolus in 2 out of 4 experimental animals (fig. 3a, b). EGFP-positive

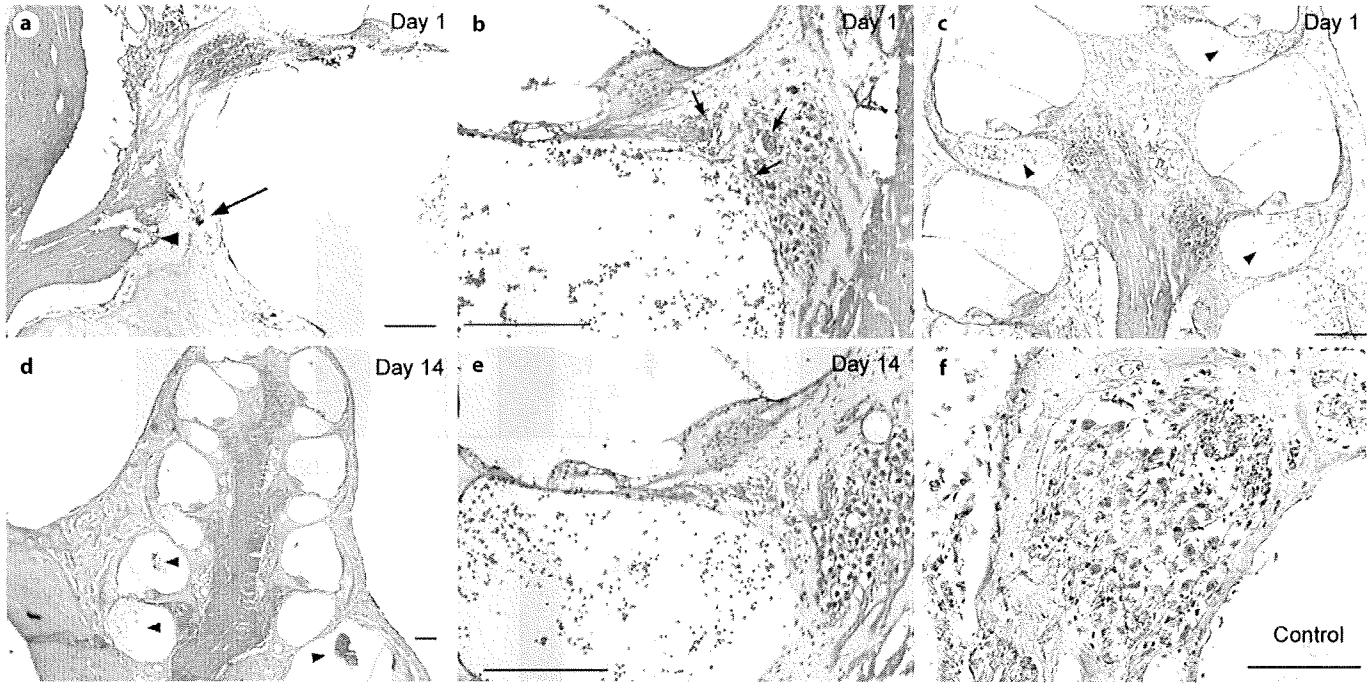

Fig. 5. Histological damage in a cochlea due to surgical procedures. **a** At the injection site, bone fracture of the cochlear modiolus (arrow) and injury of nerve fibers (arrowhead) is found on day 1 after surgery. **b** In the mid-basal portion of the cochlea on day 1 after surgery, red blood cells are observed in Rosenthal's canal (arrows). **c** From the second to the apical turn of the cochlea, no degenerative changes in the organ of Corti and spiral ganglions are identified, although a number of red blood cells are found in the scala tympani (arrowheads). **d** Cell infiltration (arrowheads) is observed in the scala tympani and scala vestibuli of the basal portion of the cochlea on day 14 after surgery. **e** In the basal turn of the cochlea on day 14 after surgery, the organ of Corti and the spiral ganglion exhibited normal morphology, despite cell infiltration in the scala tympani. **f** Spiral ganglion in the basal turn of the control cochlea. Bars = 20 μm.

cells were also observed in the scala vestibuli in 1 of the experimental animals (fig. 3c), indicating leakage of injected transplants from the cochlear modiolus.

Functional Damage due to Surgical Procedures

To evaluate the functional damage to SGNs and nerve fibers, we measured the eABRs, which are frequently used for evaluation of SGN function [11–15]. The mean values of the eABR thresholds immediately before and after surgery were 131.3 ± 18.6 and 125.0 ± 18.9 μA, respectively. On days 1 and 14 after surgery, the mean values were 100.0 ± 0.0 and 112.5 ± 12.5 μA, respectively. There were no significant differences in the eABR thresholds among the experimental groups (fig. 4), indicating that our procedure caused no severe functional damage of the SGNs.

Histological Damage due to Surgical Procedures

HE staining of mid-modiolar sections revealed actual points of injection in the cochlear modiolus. In all specimens, the injected points were located in the cochlear modiolus of the basal turn from a point slightly inferior to Rosenthal's canal (fig. 5a). On day 1 after surgery, infiltration of nucleated cells in the modiolus and injury in the nerve fibers was observed in the injected site (fig. 5a). From the basal to the second turn, a number of red blood cells were found in the scala tympani, scala vestibuli and scala media. Red blood cells were also found in Rosenthal's canal of the basal and mid-basal portions of cochleae (fig. 5b). However, organs of Corti and SGNs were well preserved in these portions of cochleae. In the apical portion of cochleae, no apparent histological damage was identified, although cell infiltration into the scala tympani and scala vestibuli was observed (fig. 5c). On day 14, red blood cells in the cochlear fluid space decreased (fig. 5d); however, cell infiltration in the scala tympani of the basal and mid-basal portions were still observed (fig. 5d, e). Remarkable degeneration of SGNs was not observed in the cochleae on day 14 in comparison with normal cochleae (fig. 5f). We quantified the histological damage to SGNs

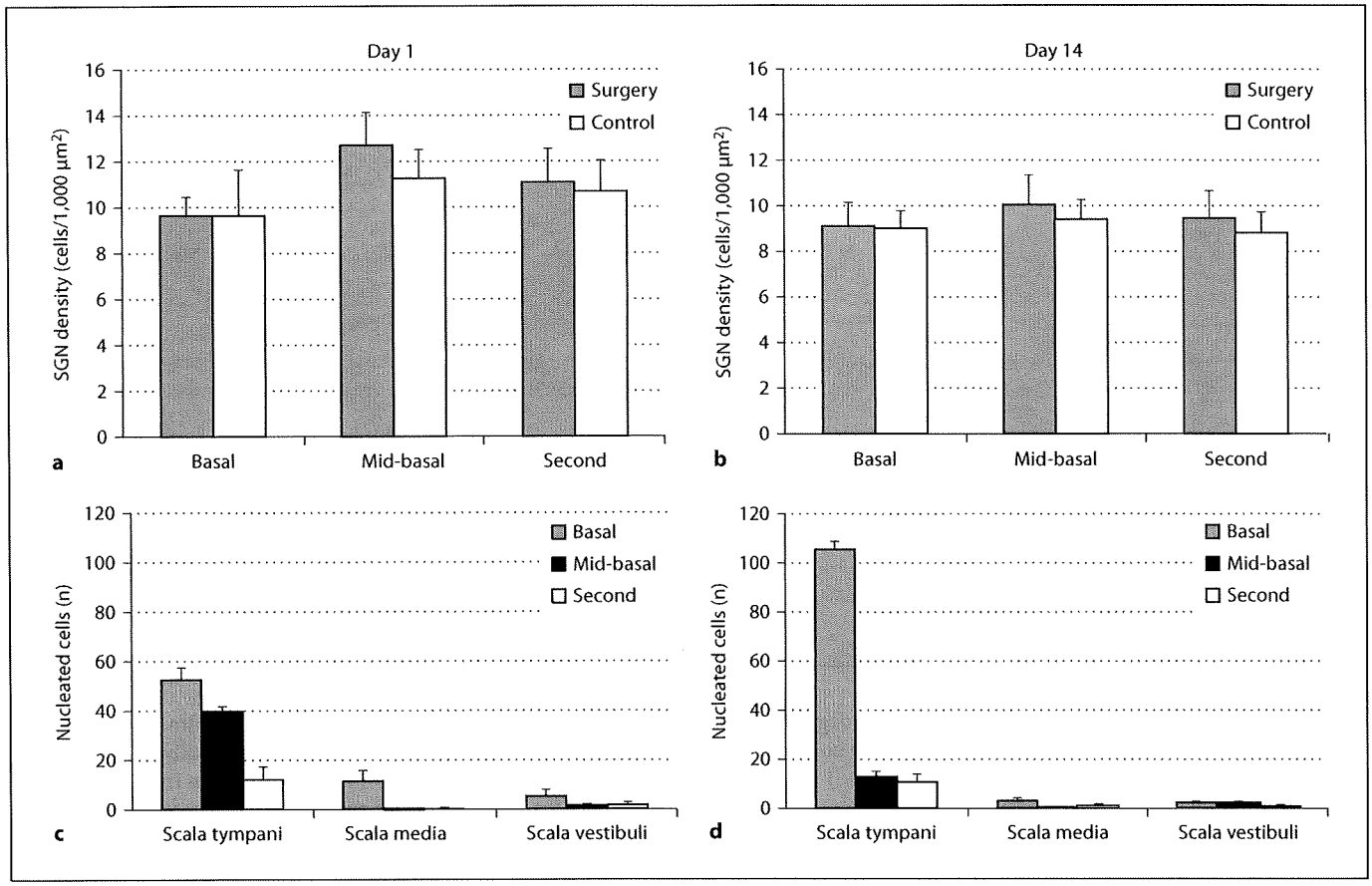

Fig. 6. Mean density of SGNs (**a**, day 1; **b**, day 14) and mean number of nucleated cells (**c**, day 1; **d**, day 14) in the basal, mid-basal and second turns of cochleae. No significant differences in the density of SGNs (SGN density) are found in each turn of cochleae between specimens after surgery and control specimens (**a**, **b**; unpaired t test). Bars show standard errors.

by measuring SGN densities in Rosenthal's canals. There were no significant differences in the SGN densities in every portion between the cochleae with surgical treatment and the cochleae without surgical treatment on days 1 or 14 after surgery (fig. 6a, b). We also quantified the number of nucleated cells in the scala tympani, scala media and scala vestibuli. A number of nucleated cells were found in the basal and mid-basal turns of the cochleae, notably in the scala tympani, on day 1 after surgery (fig. 6c). On day 14, there was a trend for the numbers of nucleated cells to decrease in the mid-basal and second turn of cochleae, while in the scala tympani of the basal turn, an increase in the number of nucleated cells was observed (fig. 6d). These findings indicate that our surgical procedure causes no significant loss of SGNs, although certain injury in the injected points and consecutive cell infiltration occurred in the basal turn of cochleae.

Discussion

The primary aim of this study was to establish a minimally invasive procedure for cell transplantation into the cochlear modiolus, which would allow for successful introduction of the transplants into the cochlear modiolus. Previously, Brown [16] established a method for recording single efferent and afferent auditory nerve cells. In this method, after cochleostomy in the basal turn of the cochlea, a small opening on the osseous spiral lamina is made using a fine insect pin followed by insertion of a fine glass electrode through the opening. This method is actually a very low invasive and efficient procedure for accessing the auditory nerves from the scala tympani. The aim of the present study was to establish a method for cell transplantation into the cochlear modioli of guinea pigs by introducing cell spheres through a glass pi-

pette. To achieve this primary aim, it is necessary to use glass pipettes with larger tips. However, the comparatively thick glass pipettes that were used in the present study were too large for insertion into the osseous spiral lamina. Therefore, we inserted a glass pipette into the modiolus of the basal portion of the cochlea.

The present findings demonstrated that there was no significant elevation of eABR thresholds after surgery, indicating that no severe functional damage of the SGNs due to surgical procedures had occurred. Measurements of eABR thresholds have frequently been used for evaluation of SGN function in animal experiments [9, 11–15]. In such experiments, animal models for severe SGN degeneration are used. Although eABR thresholds are actually effective for evaluating severe SGN degeneration, it has been reported that the eABR is of limited value when it comes to detecting only minimal SGN loss [17]. Therefore, our present findings for eABRs did not indicate that there was a complete preservation of host SGNs. We recorded eABRs immediately before and after surgery, and on days 1 and 14 after surgery in order to evaluate acute and chronic effects of our surgical procedure on ABR thresholds. The results demonstrated that there were no significant alterations in eABR thresholds between the time points for which the data were collected, indicating that the surgical procedure itself and the inflammatory responses that follow surgery do not affect eABR thresholds.

Histological analysis of the SGNs also revealed that there was no significant loss of SGNs due to our surgical procedure, which supports our present findings for eABR measurements. Although there was no significant decrease in SGNs after surgery, infiltration of nucleated cells and the presence of bleeding were found in the cochleae, mainly in the scala tympani. On day 1, nucleated cells were predominantly found in the basal and mid-basal portions of cochleae, while on day 14, the distribution of nucleated cells was limited in the basal portion of cochleae. However, the number of nucleated cells in the basal portion of cochleae on day 14 increased from that on day 1. These findings indicate that immediate inflammatory responses due to surgery occur in the basal and mid-basal portions of cochleae, and chronic inflammation continues in the basal portion until day 14. However, such inflammatory responses caused no significant SGN degeneration.

In our previous studies [9, 18], we used a 30-gauge needle for introducing transplants into the cochlear modiolus, which resulted in efficient settlement of the transplants in the cochlear modiolus. In the present study, in order to reduce the surgical invasiveness to host SGNs, a glass pipette was used for the injection of substrates into the cochlear modiolus instead of a needle. The outer diameter of a 30-gauge needle is approximately 500 μm, while that of a glass pipette is only 100 μm, which is likely to reduce the extent of surgical damage. Although the use of a glass pipette could result in an insufficient introduction of ES cell-derived neurons into the cochlear modiolus, the present histological findings demonstrated that there was an efficient settlement of transplanted cells in the cochlear modiolus. We therefore believe that the use of a glass pipette is an efficient and safe method for the introduction of cells into the cochlear modiolus of guinea pigs.

Several previous studies have documented the secretion of trophic factors from transplanted stem cells in the cochlea [19–21]. Culture media can also include various trophic factors, and thus, an injection of cell suspensions or culture media has the potential to protect SGNs against surgical invasiveness. Therefore, to evaluate surgery-related functional and histological damage to host SGNs, instead of cell suspensions, we injected saline into the cochlear modiolus.

In conclusion, our present findings demonstrate that a surgical procedure that uses a glass pipette can efficiently introduce transplants into the cochlear modiolus with no significant alteration in eABR thresholds and in SGN densities in normal adult guinea pigs. Our revised procedure for cell transplantation into the cochlear modiolus can be used to investigate the potential of various transplants for functional regeneration of SGNs in the guinea pig.

Acknowledgments

This study was supported by a Grant-in-Aid for Research on Sensory and Communicative Disorders from the Japanese Ministry of Health, Labor and Welfare, a Grant-in-Aid for Regenerative Medicine Realization, and a Grant-in-Aid for Scientific Research from the Ministry of Education, Science, Sports, Culture and Technology of Japan. The authors thank H. Niwa for providing mouse ES cells, and Y. Sasai for providing PA6 cells.

References

1 Roberson DW, Rubel EW: Cell division in the gerbil cochlea after acoustic trauma. Am J Otol 1994;15:28–34.
2 Hu Z, Ulfendahl M, Olivius NP: Central migration of neuronal tissue and embryonic stem cells following transplantation along the adult auditory nerve. Brain Res 2004; 1026:68–73.
3 Hu Z, Wei D, Johansson CB, Holmström N, Duan M, Frisén J, Ulfendahl M: Survival and neural differentiation of adult neural stem cells transplanted into the mature inner ear. Exp Cell Res 2005;302:40–47.
4 Hu Z, Ulfendahl M, Olivius NP: NGF stimulates extensive neurite outgrowth from implanted dorsal root ganglion neurons following transplantation into the adult rat inner ear. Neurobiol Dis 2005;18:184–192.
5 Sekiya T, Kojima K, Matsumoto M, Kim TS, Tamura T, Ito J: Cell transplantation to the auditory nerve and cochlear duct. Exp Neurol 2006;198:12–24.
6 Matsuoka AJ, Kondo T, Miyamoto RT, Hashino E: In vivo and in vitro characterization of bone marrow-derived stem cells in the cochlea. Laryngoscope 2006;116:1363–1367.
7 Coleman B, Hardman J, Coco A, Epp S, de Silva M, Crook J, Shepherd R: Fate of embryonic stem cells transplanted into the deafened mammalian cochlea. Cell Transplant 2006;15:369–380.
8 Corrales CE, Pan L, Li H, Liberman MC, Heller S, Edge AS: Engraftment and differentiation of embryonic stem cell-derived neural progenitor cells in the cochlear nerve trunk: growth of processes into the organ of Corti. J Neurobiol 2006;66:1489–1500.
9 Okano T, Nakagawa T, Endo T, Kim TS, Kita T, Tamura T, Matsumoto M, Ohno T, Sakamoto T, Iguchi F, Ito J: Engraftment of embryonic stem cell-derived neurons into the cochlear modiolus. Neuroreport 2005;16: 1919–1922.
10 Kawasaki H, Mizuseki, K, Nishikawa S, Kaneko S, Kuwana Y, Nakanishi S, Nishikawa SI, Sasai Y: Induction of midbrain dopaminergic neurons from ES cells by stromal cell-derived inducing activity. Neuron 2000; 28:31–40.
11 Endo T, Nakagawa T, Kita T, Iguchi F, Kim TS, Tamura T, Iwai K, Tabata Y, Ito J: Novel strategy for treatment of inner ears using a biodegradable gel. Laryngoscope 2005;115: 2016–2020.
12 Hall RD: Estimation of surviving spiral ganglion cells in the deaf rat using the electrically evoked auditory brainstem response. Hear Res 1990;45:123–136.
13 Shinohara T, Bredberg G, Ulfendahl M, Pyykkö I, Olivius NP, Kaksonen R, Lindström B, Altschuler R, Miller JM: Neurotrophic factor intervention restores auditory function in deafened animals. Proc Natl Acad Sci USA 2002;99:1657–1660.
14 Yamagata T, Miller JM, Ulfendahl M, Olivius NP, Altschuler RA, Pyykkö I, Brendberg G: Delayed neurotrophic treatment preserves nerve survival and electrophysiological responsiveness in neomysin-deafened guinea pigs. J Neurosci Res 2004;78:75–86.
15 Maruyama J, Yamagata T, Ulfendahl M, Brendberg G, Altschuler RA, Miller JM: Effects of antioxidants on auditory nerve function and survival in deafened guinea pigs. Neurobiol Dis 2006;25:309–318.
16 Brown MC: Morphology and response properties of single olivocochlear fibers in the guinea pig. Hear Res 1989;40:93–109.
17 Smith L, Simmons FB: Estimating eighth nerve survival by electrical stimulation. Ann Otol Rhinol Laryngol 1983;92:19–23.
18 Naito Y, Nakamura T, Nakagawa T, Iguchi F, Endo T, Fujino K, Kim TS, Hiratsuka Y, Tamura T, Kanemaru S, Shimizu Y, Ito J: Transplantation of bone marrow stromal cells into the cochlea of chinchillas. Neuroreport 2004;15:1–4.
19 Iguchi F, Nakagawa T, Tateya I, Kim TS, Endo T, Taniguchi Z, Naito Y, Ito J: Trophic support of mouse inner ear by neural stem cell transplantation. Neuroreport 2003;14: 77–80.
20 Hakuba N, Hata R, Morizane I, Feng G, Shimizu Y, Fujita K, Yoshida T, Sakanaka M, Gyo K: Neural stem cells suppress the hearing threshold shift caused by cochlear ischemia. Neuroreport 2005;16:1545–1549.
21 Yoshida T, Hakuba N, Morizane I, Fujita K, Cao F, Zhu P, Uchida N, Kameda K, Sakanaka M, Gyo K, Hata R: Hematopoietic stem cells prevent hair cell death after transient cochlear ischemia through paracrine effects. Neuroscience 2007;145:923–930.

JOHNS
特集●耳の奇形●

症状・診断

内耳奇形の聴覚検査所見

熊川孝三*
Kozo KUMAKAWA

● Key Words ●内耳奇形，前庭水管拡大症，内耳道狭窄症●

はじめに

骨迷路の形態異常を伴う内耳奇形の頻度は一般に考えられているよりも高く，Jensen[1]は先天性高度感音難聴者の20％に認められると報告している。その分類には多くのものがある。

病理組織学的には，

1）Michel型：内耳の完全欠損
2）Mondini型：骨迷路，膜迷路が不完全に発育
3）Bing-Siebenmann型：骨迷路は正常で膜迷路，感覚細胞が不完全に発育
4）Scheibe型：蝸牛の膜迷路と球形嚢に障害があるが前庭膜迷路と骨迷路は正常に発育

などと分類されることが多い。しかし，このような分類は病理組織学的検査によって初めて可能になるもので，実際の画像・臨床診断には適さない。

そこでJackler ら[2]はこれらの点を考慮して**表1**のような分類を提唱している。これは，まず，膜迷路に限局した奇形と，骨迷路と膜迷路の異常を合併するものに大きく分け，さらに後者を，

A：内耳の無形成
B：蝸牛奇形を伴うもの
C：蝸牛の異常を伴わず半規管・前庭の迷路奇形のみを伴うもの
D：水管の奇形
E：内耳道の奇形

とに分ける分類である。これらの分類は画像診断の所見に基づいており，臨床診断に適している。ここではこの分類にしたがって内耳奇形を分類し，それぞれの聴覚検査所見について述べる。

表1　内耳奇形の分類（Jackler ら）[2]

Ⅰ．膜迷路に限局した奇形
　A．膜迷路の完全異形成
　B．膜迷路の限局した異形成
　　1）蝸牛，球形嚢の異形成（Scheibe）
　　2）蝸牛基底回転の異形成（Alexander）
Ⅱ．骨迷路と膜迷路の奇形
　A．迷路の無形成（Michel）
　B．蝸牛の奇形
　　1）蝸牛の無形成
　　2）蝸牛の低形成
　　3）骨隔壁の低形成（Mondini）
　　4）共通腔（common cavity）
　C．迷路奇形
　　1）半規管異形成
　　2）半規管無形成
　D．水管の奇形
　　1）前庭水管拡大
　　2）蝸牛水管拡大
　E．内耳道の奇形
　　1）内耳道狭窄
　　2）内耳道拡大

Ⅰ．内耳奇形の型と聴力像

Jackler らの分類[2]にしたがって，彼らの聴力レベルの解析結果を**表2**に示す。**図1**は蝸牛の異常を伴う内耳奇形について，**図2**は蝸牛の異常を伴わない半規管・前庭の内耳奇形について，筆者[3]が改変し，それぞれ発達が停止した胎生時期順に示した。

Michel型は内耳の完全欠損であり，当然ながら聴力はスケールアウトである。

Bの蝸牛奇形を伴う群の中で最も頻度が高いものは，一般的にMondini型奇形と呼ばれている奇

* 虎の門病院耳鼻咽喉科・聴覚センター
〔〒105-8470 東京都港区虎ノ門2-2-2〕

表 2　内耳奇形の分類と平均聴力（Jackler ら）[2]

型	耳数	0～40	41～80	81～100	101～120	>120 dB *
A 内耳の完全欠損（Michel）	1	—	—	—	—	1
B 蝸牛奇形を伴うもの						
蝸牛・前庭が共通腔	19	1	6	—	3	9
蝸牛無形成	2	—	—	—	1	1
蝸牛低形成	11	6	3	1	—	1
蝸牛回転の隔壁欠損（Mondini）	41	7	15	4	7	8
C 蝸牛奇形を伴わないもの						
前庭・半規管の形成不全	7	5	—	1	1	—
D 前庭水管の拡大	17	7	4	4	2	—

＊ 500，1000，2000 Hz の平均聴力

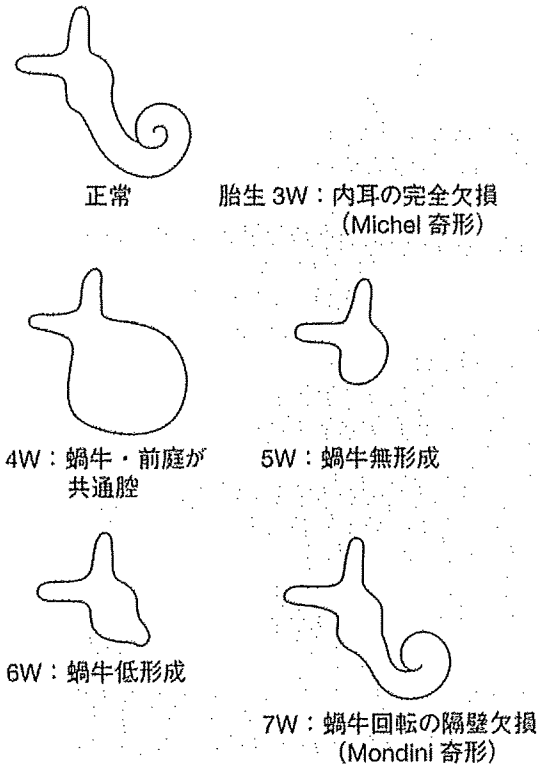

図 1　蝸牛の異常を伴う内耳奇形（Jackler[2] より改変）[3]
発達が停止した胎生時期を示す。

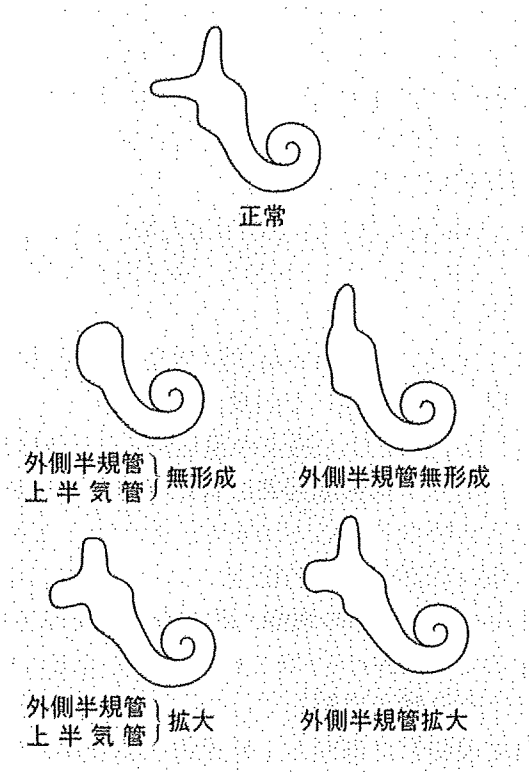

図 2　蝸牛の異常を伴わない内耳奇形（Jackler[2] より改変）[3]
胎生 6 週～22 週における発達の停止による。

形である。これは，胎生 7 週目の異常で，蝸牛軸が不完全で基底回転（第 1 回転）までは発達しているが，それよりも distal の回転間の隔壁が欠損し，中・頂回転が合わさって嚢状に置き換わったものである。コルチ器・有毛細胞と聴神経終末の欠損程度にはバラツキがあり，**表 2** に示したように難聴も軽度から高度までさまざまである。

次に多いのは胎生 4 週目の異常で，蝸牛と前庭が大きな共通した腔となって蝸牛の回転が形成されていない共通腔 common cavity 型と呼ばれているものである。聴力は表 2 に示すように不良なものが多いが，意外にも中等度の低下にとどまるものもある。

次いで，蝸牛低形成型では聴力低下は軽度のものが多いことがわかる。

C の蝸牛の異常を伴わない半規管・前庭の内耳

奇形は，表2に示したように，蝸牛形態が正常であるために，聴力低下も軽度なものが多いが，一方，高度な難聴を伴うこともある。

Dの前庭水管拡大を伴う奇形では聴力低下は軽度なものから高度まで幅広く分布し，変動性であり，また，低音域の気骨導差の存在が認められることが多い。このために聴力レベルの割に補聴効果が出やすいことが特徴的な点としてあげられる。

II．内耳奇形の型とラセン神経節の残存

内耳奇形でも型によってはラセン神経節がある程度数は形成されていることは組織学的にも確認されている。Jackler ら[4]は共通腔型の2耳，蝸牛低形成の2耳，Mondini 型奇形の1耳の計5耳に初めて単チャンネル方式人工内耳を埋め込み，音知覚を生ず得ることを確認した。以来，多チャンネル方式の人工内耳についても内耳奇形で有効であることが多数報告されている。

Schmidt[5]によれば，正常人のラセン神経節数は25,000から35,000であるのに対し，Mondini 型内耳奇形では7,677から16,110，平均11,478であったと報告している。さらにラセン神経節は共通腔奇形や蝸牛軸形成不全の奇形ではその耳胞壁に存在していると報告した。したがってこれらの内耳奇形でも必ずしも人工内耳が無効ではないと考えられる。ただし，周波数情報を十分に伝えるには，蝸牛の回転がある程度形成されている奇形，すなわちMondini 型奇形の方が共通腔型奇形よりも聴取成績の点では有利であろう。Michel 型奇形および蝸牛無形成の場合にはラセン神経節の形成もなく，人工内耳の適応とはならない。

III．前庭水管拡大症(Large vestibular aqueduct syndrome，以下 LVAS と略す)

1．概　説

1978年に Valvassori と Clemis[6]によって報告された内耳奇形であり，内リンパ嚢と前庭水管の拡大を特徴とする。CT，MRI など画像診断が先天性難聴児の画像診断に用いられるようになってから発見頻度は増え，内耳奇形の中でも最も頻度の高い奇形であるとされている[7]。

側頭骨の高分解能 CT では拡大した前庭水管が

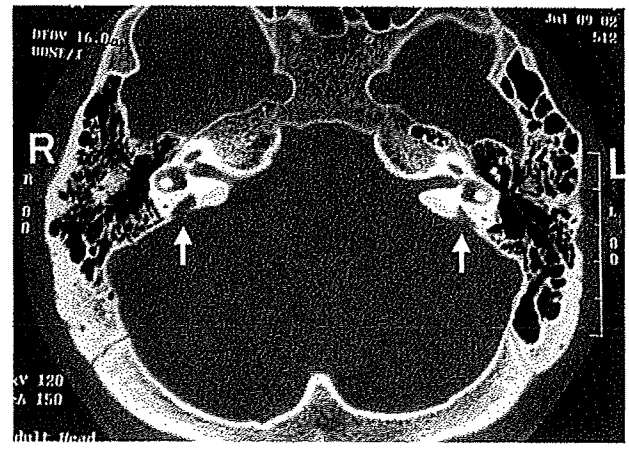

図 3　前庭水管拡大症の CT スキャン
矢印：拡大した両側の前庭水管を示す。

前庭に直結している所見が認められる（図3）。合併する奇形として，半規管の異常，拡大した前庭，Mondini 奇形の合併などがある。

2．症　状

小児期に発症して，時に頭部の外傷を契機として，めまい発作を反復しながら次第に進行し，ついには高度難聴となる難治性疾患として知られている。

3．遺伝学的異常

本疾患は常染色体劣性遺伝であり，Abe ら[8]は7番染色体長腕（7q31）に原因遺伝子が存在することを報告した。この領域は先天性感音難聴と甲状腺腫を伴う Pendred 症候群の原因遺伝子である PDS 遺伝子の存在する領域であるが，Usami ら[9]は PDS 遺伝子が同時に LVAS の原因遺伝子であることを明らかにし，両者は PDS 遺伝子変異による表現型が異なる一連の疾患群であることを報告した。

4．聴覚検査所見

46～65％に小児期の難聴があり，15～25％に低音域の気骨導差の存在が認められるという[10]。低音域における気導骨導差の存在に対しては明白な機序は不明であるが，内リンパ圧の上昇によるアブミ骨の可動性の低下も一因として推測される。

内耳障害の機序としては拡大した前庭水管を通

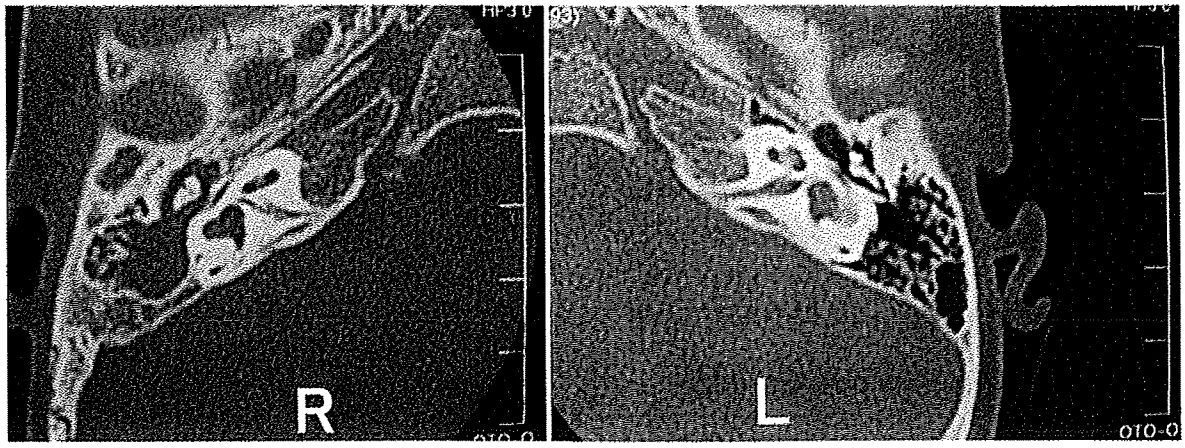

図 4　両側内耳道狭窄症の側頭骨 CT
右滲出液の貯留，外側半規管の奇形および両側内耳道の狭窄が認められる。

じて脳圧が内耳に伝わり，内耳の症状を誘発するものと考えられる。悪化に頭部外傷が契機となることはこれを裏付ける。時には膜迷路が破綻し，急激な聴力低下をきたし，最終的にはコルチ器の障害をきたすものと推測される。しかし，進行性の内耳障害をきたす他の因子の存在も否定できず，複数の機序が存在する可能性もある。

5．治　療

急性増悪時には突発性難聴に準じた副腎皮質ステロイド投与が行われ，ほとんどの例で奏効する。通常，1〜2 週間の投与で回復することが多い。しかし，頻回のめまい発作例では副作用のために投与を中止せざるを得ない例も多い。また長期的には次第に聴力が悪化するのを阻止できない場合が多く，最終的に人工内耳の適応となる例も多い。

これまでに LVAS 症例の拡大した内リンパ嚢を充填する手術が行われて，これを無効とする報告[10]と，有効とする Wilson ら[11]，内藤ら[12]の報告がある。

われわれは，乳突洞削開後に細い硬性内視鏡を硬膜と側頭骨の間に入れて空間を確保し，内リンパ嚢が側頭骨内に入ってゆく部位を確認し，そこでチタン製クリップを用いて内リンパ嚢をクリッピングする新しい術式を考案した[13,14]。本術式は内リンパ嚢の切開を行わずに済み，また圧迫による内リンパ圧の急激な上昇も避けられ，内耳に対する侵襲がこれまでの術式に比べて少なく，聴力保存については内リンパ嚢充填術よりも小侵襲のクリッピング術が有利であった。進行性に 80 dB 程度まで悪化し，かつ，保存治療で改善が期待できなくなった場合には外科的療法の 1 つとして試みられて良いと考える。

Ⅳ．内耳道奇形

1．概　説

ときに先天奇形あるいはクモ膜嚢胞による内耳道拡大が認められることがあるが，この場合，聴力は正常であることが多い。

先天性の内耳道狭窄は蝸牛前庭神経の形成不全が二次的に内耳道の狭窄を引き起こすと考えられている[15]。両側内耳道狭窄症は極めて稀である[16]。両側内耳道狭窄症例の側頭骨 CT を図 4 に示す。

2．内耳道狭窄症の聴覚検査所見

ほとんどの例で聴神経の低形成に伴う高度難聴が認められる。基本的に両側内耳道狭窄症は画像から診断がなされることがほとんどであり，最終的に人工内耳の適応決定，有効性予測の判断が問題となる。

画像診断で高度の両側内耳道狭窄症例あるいは内耳奇形が認められる症例に対して，われわれが行う聴覚検査ならびに画像診断のフローチャートを図 5 に示す。

BOA，CORの聴性行動反応検査，ABR，聴性定常反応検査（ASSR：auditory steady-state response）などの検査で聴覚反応がある程度認められた場合，一般的には純音聴力検査の閾値が100 dB未満で補聴器装用閾値が60 dB未満であれば補聴器の適応である。一方，高度難聴でも聴覚反応がわずかにあり，かつMRIで蝸牛神経が明らかに確認できれば，電気刺激ABR（EABR）を施行せずとも人工内耳適応ありとして問題ない。

しかし，聴覚反応がほとんどなく，さらにはMRIで聴神経が同定困難である場合には最終的には全身麻酔下で鼓膜から電極刺入し，これによる電気刺激ABR（electrically induced ABR：EABR）を行うことで適応を決定する。高橋，熊川ら[17]はEABRで反応が認められた両側内耳道狭窄症例に人工内耳埋め込み手術を行い，その有効性を報告した。

V．当院の高度難聴乳幼児の精密聴力検査システム

現在，難聴が疑われる乳児・幼児では，通常は聴性行動反応聴力検査（BOA），条件詮索反射聴力検査（COR），聴性脳幹反応検査（ABR）を行う。しかし行動観察方式の問題点として適応年齢，再現性，左右別の閾値測定が困難，重複障害児における正確さの問題がある。またABRの問題点としてクリック音を使うために低音域の聴力が反映されず，補聴器の装用効果を予測しにくいという難点がある。このため対象児の年齢が小さくなればなるほど，耳鼻咽喉科医は難聴の程度と聴力像の提示に難渋しているのが現状である。

また，画像検査も必要であり，各検査毎に通院と睡眠剤の投与を行うのは，患児，両親，医師のいずれにとっても負担であった。

そこで，われわれは乳幼児の精密聴力検査のシステムとして，周波数特性を持ち，かつ他覚的な聴力検査である蝸電図検査（electrocochleography：ECoG），聴性定常反応検査（ASSR）に加えて，岬角電気刺激によるEABRとCT，MRIも組み合わせて，短期間の入院で乳幼児の検査を効率的に行うシステムを考案し，同一小児群を対象にした検討で以下の結果を得た[18]。

1）鼓室内誘導法によるECoGとASSR検査を行うことでABR無反応耳の82％において低音域周波数の域値測定が可能となった。

2）鼓室内誘導法によるECoGはASSRよりも反応閾値は5～15 dB低く，その差は低音域ほど大きく，ECoGの反応検出率はASSRの2倍高かった。

3）EABRは聴覚反応の得られない内耳道狭窄例など蝸牛神経の形成不全が考えられる例ではきわめて有効な人工内耳の適応決定手段と考えられた。

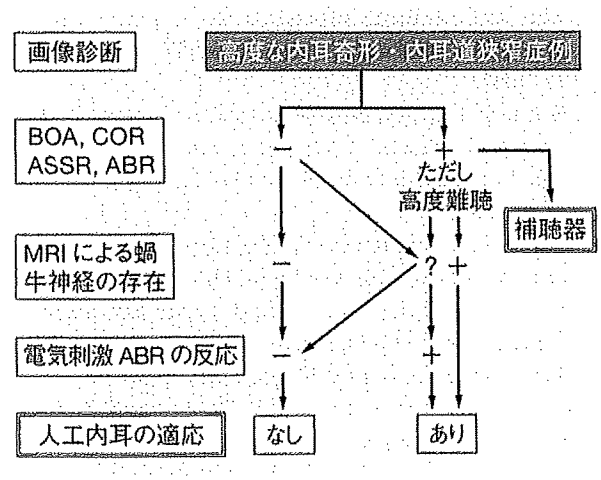

図5　高度な内耳奇形・内耳道狭窄症の検査フローチャート

おわりに

内耳奇形の診断には聴覚検査のみならず，画像検査，遺伝学的検査も併せて行い，EABR検査が人工内耳の適応と有効性を予測する上で有用であることを述べた。

本研究は平成20年度厚生労働科学研究費補助金によって行われた。

文　献

1) Jensen J：Malformation of the inner ear in deaf children. Acta Radio (Suppl 286)：1-97, 1969.
2) Jackler RK, Luxford WM, House WF：Congenital malformation of the inner ear；A classification based on embryogenesis. Laryngoscope 97 (Suppl 40)：2-14, 1987.
3) 熊川孝三：幼少児難聴の画像診断―内耳奇形と人工内耳―．耳鼻と臨床 40：95-99，1994.
4) Jackler RK, Luxford WM, House WF：Sound detec-

tion with cochlear implant in five cases of four children of the cochlea. Laryngoscope 97 (suppl 40) : 15-17, 1987.
5) Schmidt JM : Cochlear neuronal populations in developmental defects of the inner ear ; Implications for cochlear implantation. Acta Oto-Laryngologica 99 : 14-20, 1985.
6) Valvassori GE, Clemis JD : The large vestibular aqueduct syndrome. Laryngoscope 88 : 723-748, 1978.
7) Smith SD, Harker LA : Single gene influences on radiologically-detectable malformations of the inner ear. J Commun Disord 31 : 391-410, 1998.
8) Abe S, Usami S, Shinkawa H : Three familial cases of hearing loss associated with enlarged vestibular-aqueduct maps to 7q31, the region containing the Pendred gene. Am J Med Genet 82 : 322-328, 1999.
9) Usami S, Abe S, Weston MD, et al : Non-syndromic loss associated with enlarged vestibular aqueduct is caused by PDS mutations. Hum Genet 104 : 188-192, 1999.
10) Zalzal GH, Thomaski SM, Vezina LG, et al : Enlarged vestibular aqueduct and sensorinueral hearing loss in childhood. Arch Otolarungol Head Nech Surg 121 : 23-28, 1995.
11) Wilson DF, et al : Endolymphatic sac obliteration for large vestibular aqueduct syndrome. Am J Otol 18 : 101-107, 1997.
12) 内藤　泰，髙橋晴雄：前庭水管の手術について．耳鼻臨床 93：802-803，2000.
13) 熊川孝三，髙橋優宏，武田英彦，他：前庭水管拡大症に対する内視鏡使用による内リンパ嚢クリッピング術．Otol Jpn 13：251，2003.
14) 熊川孝三，宇佐美真一：前庭水管拡大症．JOHNS 21 (9)：1199-1201，2005.
15) Nelson EG, Hinojosa R : Aplasia of the cochlear nerve ; A temporal bone study. Otol Neurotol 22 : 790-795, 2001.
16) Camacho RR, Berrocal JRG, Arellano B : Bilateral malformation of the internal auditory canal ; Atresia and contralateral transeverse megacrest. Otolaryngol Head Neck Surg 125 : 115-116, 2001.
17) 髙橋優宏，熊川孝三，武田英彦，他：人工内耳埋め込みが有効であった両側内耳道狭窄頭の1症例．Otol Japan 14：248-251，2004.
18) 熊川孝三，鈴木久美子，武田英彦，他：短期入院による乳幼児の他覚的精密聴力検査ーシステムの紹介およびABR，蝸電図，聴性定常反応，EABRの検討ー．Audiology Japan 48：156-164，2005.

*　　*　　*

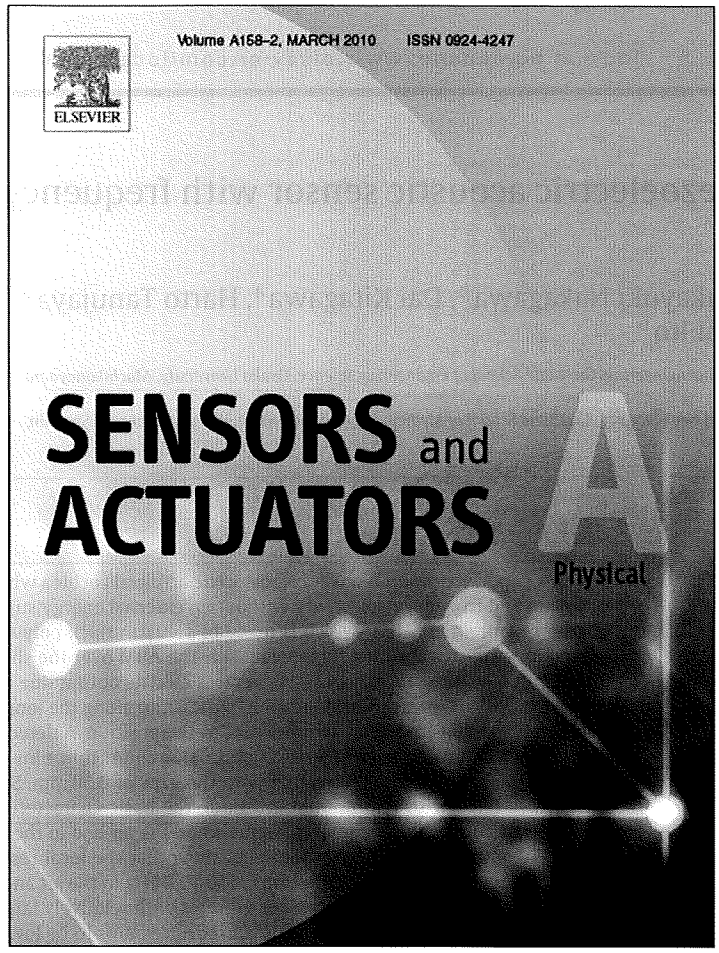

Sensors and Actuators A 158 (2010) 183–192

Contents lists available at ScienceDirect

Sensors and Actuators A: Physical

journal homepage: www.elsevier.com/locate/sna

Development of piezoelectric acoustic sensor with frequency selectivity for artificial cochlea

Hirofumi Shintaku[a,*], Takayuki Nakagawa[b], Dai Kitagawa[a], Harto Tanujaya[a], Satoyuki Kawano[a], Juichi Ito[b]

[a] Department of Mechanical Science and Bioengineering, Graduate School of Engineering Science, Osaka University, Machikaneyama-cho 1-3, Toyonaka, Osaka 560-8531, Japan
[b] Department of Otolaryngology, Head and Neck Surgery, Graduate School of Medicine, Kyoto University, Kawahara-cho 54,Shogoin, Sakyo-ku, Kyoto 606-8507, Japan

ARTICLE INFO

Article history:
Received 25 July 2009
Received in revised form
13 November 2009
Accepted 22 December 2009
Available online 4 January 2010

Keywords:
Fluid-structure interaction
Acoustic MEMS sensor
Artificial cochlea
Biomechanical engineering
Piezoelectric device

ABSTRACT

In this paper, we report a novel piezoelectric artificial cochlea which realizes both acoustic/electric conversion and frequency selectivity without an external energy supply. The device comprises an artificial basilar membrane (ABM) which is made of a 40 μm thick polyvinylidine difluoride (PVDF) membrane fixed on a substrate with a trapezoidal slit. The ABM over the slit, which mimics the biological system, is vibrated by acoustic waves and generates electric output due to the piezoelectric effect of PVDF. The width of ABM is linearly varied from 2.0 to 4.0 mm along the longitudinal direction of 30 mm to change its local resonant frequency with respect to the position. A detecting electrode array with 24-elements of 0.50 × 1.0 mm rectangles is made of an aluminum thin film on ABM, where they are located in a center line of longitudinal direction with the gaps of 0.50 mm. Since the device will be implanted into a cochlea filled with lymph fluid in future, the basic characteristics in terms of vibration and acoustic/electric conversion are investigated both in the air and in the silicone oil which is a model of lymph fluid. The in vitro optical measurements show that the local resonant frequency of vibration is varied along the longitudinal direction from 6.6 to 19.8 kHz in the air and from 1.4 to 4.9 kHz in the silicone oil, respectively. Since a resonating place vibrates with relatively large amplitude, the electric output there becomes high and that at the other electrodes remains to be low. Thus, the electric voltages from each electrode realize the frequency selectivity. Furthermore, the effect of surrounding fluid on the vibration is discussed in detail by comparing the experimental results with the theoretical predictions obtained by the Wentzel–Kramers–Brillouin asymptotic method. The theoretical prediction indicates that the surrounding fluid of the higher density induces the larger effective mass for the vibration that results in lower resonant frequency. From these findings, the feasibility of artificial cochlea is confirmed both experimentally and theoretically.

1. Introduction

The sensorineural hearing loss is a type of deafness which is often caused by the damage on hair cells of cochleae in inner ears. The hair cells convert acoustic sounds to electric signals that stimulate auditory nerves. As a clinical treatment for the hearing loss in children and adults, the artificial cochlea is recently well used. The device bypasses the damaged hair cells by generating the electric current in response to the acoustic sound [1,2]. The current artificial cochlea consists of an implantable electrode array for the stimulation and an extracorporeal device including a microphone, a sound processor and a battery. The acoustic sound is detected and is analyzed with respect to the frequency by the extracorporeal device. The processed signals are transferred through a transcutaneous system. Then, the auditory nerves are stimulated through the electrodes inserted in the cochlea. The disadvantages in the current system are the indispensability of extracorporeal devices, the small number of electrodes which closely connects to the limitation of tones, and the relatively large power consumption. This situation motivates us to develop a fully self-contained implantable artificial cochlea.

The important functions of cochlea are not only the conversion of acoustic wave to electric signals but also the frequency selectivity [3,4]. The basilar membrane which is a biological diaphragm in the cochlea plays an important role for the frequency selectivity. The local eigen frequency of membrane is changing along the place

* Corresponding author. Tel.: +81 6 6850 6179; fax: +81 6 6850 6179.
E-mail address: shintaku@me.es.osaka-u.ac.jp (H. Shintaku).

0924-4247/$ – see front matter © 2009 Elsevier B.V. All rights reserved.
doi:10.1016/j.sna.2009.12.021

Nomenclature

A_j	Fourier coefficient
$b(x)$	width of ABM, m
D	bending rigidity, N m
E	Young's modulus, Pa
f	frequency, Hz
h	thickness of ABM, m
$k(x)$	wave number, m^{-1}
L_1	width of fluid channel, m
L_2	depth of fluid channel, m
L_3	length of ABM, m
p_f	pressure, Pa
w	displacement of ABM, m
$W(x)$	envelope function, m
(x, y, z)	Cartesian coordinates, m

Greek letters

$\eta(x, y)$	shape function for ABM's bending in y direction
ν	Poisson ratio
ρ_f	density of fluid, kg m^{-3}
ρ_m	density of PVDF, kg m^{-3}
$\phi_f(x, y, z, t)$	velocity potential, m^2/s
ω	angular frequency, rad/s

Subscripts

f	region of fluid channel f = l or u
j	mode number of Fourier coefficient
l	lower fluid channel
m	PVDF
u	upper fluid channel

of it, because of varying mechanical boundary conditions and the mechanical rigidity. Thus, when the eigen frequency at a local place match to that of acoustic wave, the place vibrates with relatively large amplitude due to the resonance. The vibration stimulates hair cells especially at the resonated place. As a result, the frequency of acoustic wave is recognized as the difference in tones.

To artificially realize the frequency selectivity, some microscaled devices have been reported. Tanaka et al. [5] and Xu et al. [6] developed acoustic sensors with the function of frequency selectivity by the use of resonance of cantilever arrays. Those sensors were evaluated in the atmospheric environment. Chen et al. [7] developed a beam array fixed on a trapezoidal channel and investigated the vibrating characteristics in the water. Despite the frequency selectivity of cantilevers or beams, their mechanical strength may not be enough for the implantation as the artificial cochleae for the long period. On the other hand, White and Grosh [8] developed a device made of polyimide membrane with Si_3N_4 beams. The demonstration for the frequency selectivity was conducted at the higher frequency range compared with the audible one. Wittbrodt et al. [9] also developed a device made of polyimide membrane with Al beams. They reported that the device possessed some similarities with the biological cochlea in terms of traveling waves, the frequency to place tonotopic organization, and the roll off beyond the characteristic place.

The acoustic sensor which is developed in this paper realizes both the frequency selectivity and the conversion of acoustic wave to the electric signal in the liquid environment without an external energy supply. The device is designed as a prototype model to test the basic concept of the acoustic sensor for the development of the self-contained implantable artificial cochlea. The device consists of a piezoelectric membrane fixed on a trapezoidal slit, where the membrane over the slit works as a detector. We name this trapezoidal membrane as an artificial basilar membrane (ABM). Discrete electrodes are fabricated on ABM by technologies of micro electromechanical systems (MEMS) to measure the electric signals generated in response to the externally applied acoustic waves. To model the liquid environment, the fluid channel which locates under ABM is filled with a silicone oil as a model of lymph fluid in the cochlea. The ABM's vibration is measured using a laser Doppler vibrometer (LDV) at the various frequencies in the range of 1.0–20 kHz. The electric output is measured through the electrodes using a preamplifier. To predict the performance of the present device, the oscillatory dynamics of ABM is theoretically analyzed based on the vibrating equation of a thin plate bending and equations for the fluid dynamics. The phenomenon of fluid-structure interaction is treated by coupling those basic equations. To treat the wave motion on trapezoidal ABM, the Wentzel–Kramers–Brillouin (WKB) asymptotic solution [10] is used under the assumption of the gradually varying wavelength. The comparison between the experimental and theoretical results makes clear the detailed mechanism underlying the frequency selectivity. In addition, discussions for the further development as an implantable artificial cochlea are described from the viewpoint of magnitude of electric signal and the device size.

2. Principles and experimental methods

2.1. Basic mechanism of frequency selectivity and electric signal generation

A schematic and a photograph of piezoelectric acoustic sensor developed here are shown in Fig. 1. The device comprises a polyvinylidine difluoride (PVDF) membrane (KUREHA, Japan) bonded on a stainless plate with a trapezoidal slit and discrete electrodes distributed along x axis. PVDF is a piezoelectric material which can convert mechanical stresses to electric signals. The trapezoidal slit is designed so that the membrane over it, i.e. ABM, can be easily vibrated by the acoustic wave. The width $b(x)$ of ABM is linearly varied in the ranges of 2.0–4.0 mm along x of 30 mm long. This shape is intended to mimic the passive basilar membrane, that is, the local resonant frequency (LRF) of ABM gradually changes due to the varying mechanical boundary conditions along x. LRF is expected to be decreased as x increases. Applying acoustic wave with a certain frequency to ABM, a local place vibrates with relatively large amplitude due to the resonance. Electric signals are generated by the piezoelectric effect with respect to the local stress in ABM. Thus, the electrode on the resonating place gives a relatively large electric output. This is the basic mechanism of frequency selectivity realized by the association of resonance of vibration and the discrete electrode array. The device is mounted on a substrate with a fluid channel, where the channel dimensions are 47 × 17 mm rectangle and 4 mm deep. To model an in vivo environment, the fluid channel is filled with silicone oil (Shin-Etsu Chemical, Japan). The density and the viscosity of silicone oil are 873 kg/m^3 and 1.75×10^{-3} Pa s, respectively, where those of lymph fluid in cochleae are typically reported as 1.0×10^3 kg/m^3 [11] and from 1.0×10^{-3} to 1.97×10^{-3} Pa s [12,13], respectively. Although the both sides of basilar membrane in vivo face to the lymph fluid, in this experiment, only the bottom side of ABM faces to the silicone oil for the stable optical measurement from the upper side. The effect of this simplification is discussed by the theoretical analysis in the later section. Furthermore, the size of this ABM is relatively large to be implanted into the human cochlea. However, the main purpose of this paper is to test the basic mechanism of proposed system in terms of acoustic/electric conversion and the frequency selectivity. The optimization and the miniaturization will be remained as a future work. The advantages of miniaturized ABM are again discussed in later section.

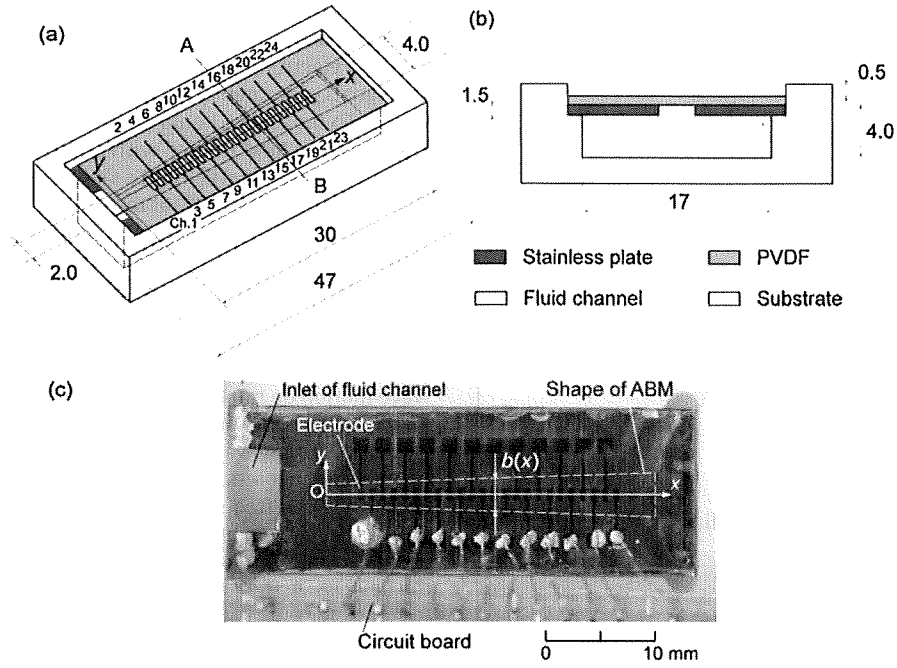

Fig. 1. Schematic and photograph of piezoelectric acoustic sensor; (a) 3D view, (b) cross sectional view at AB, and (c) photograph (Unit: mm).

2.2. Experimental setup

The electrode array with 24 elements made of an aluminum thin film is fabricated on an upper side of a 40 μm thick PVDF membrane based on a standard photolithography and an etching process. For convenience, the electrodes are named as Ch.1–Ch.24 as shown in Fig. 1(a). The each electrode of 0.50 × 1.0 mm rectangular shape is equally spaced 1.0 mm center to center, resulting in a gap of 0.50 mm between two adjacent electrodes. The ground electrode is prepared as a common one for all discrete electrodes on the lower side of ABM. The membrane is glued on the stainless plate to be the trapezoidal ABM. Since the electrodes of about 100 nm thick are extremely thinner than the PVDF of 40 μm, they may not strongly affect on the vibrating characteristics of ABM.

Fig. 2 shows a schematic of experimental setup. The sinusoidal acoustic wave is applied to the device from a speaker (FOSTEX, Japan) which is located 120 mm distant with 45° at a tilt. The speaker is previously calibrated to realize the constant sound pressure with the precision of ±0.1 dBSPL at various frequencies. The frequency is controlled by the function generator (NF, Japan) from 1.0 to 20 kHz which is in the range of audible frequency. The device on the substrate is set on a motorized stage which moves x and y directions for the measurement of spatial distribution of vibration amplitude. The velocity of ABM in z due to the vibration by the acoustic wave is measured by the LDV (Graphtec, Japan). The displacement, which is converted from the velocity data, is analyzed by an FFT to obtain the amplitude of vibration at the frequency of acoustic wave. At the same time, the piezoelectric output from the electrodes is measured in terms of voltage using a preamplifier and an oscilloscope.

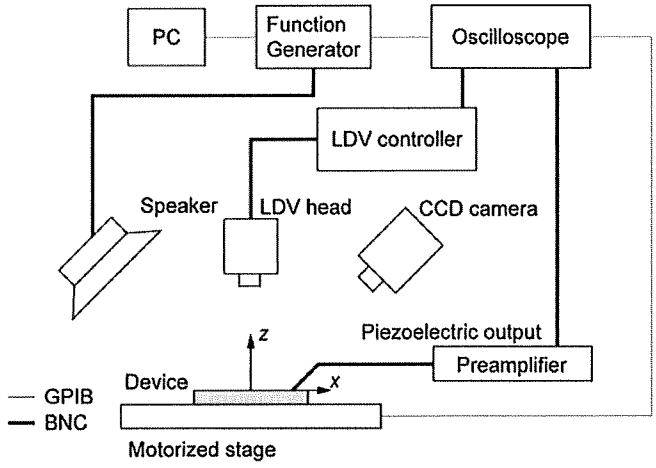

Fig. 2. Schematic of experimental setup for measurement of vibrating characteristics of ABM.

2.3. Oscillatory dynamics of artificial basilar membrane

Because the phenomena including the fluid-structure interaction are relatively complex, it is important for practical engineering to develop a theoretical model that effectively and easily predicts the vibrating characteristics of ABM. To obtain a mathematical solution, the following assumptions are made based on the experimental observations.

(1) The vibration of ABM is modeled as the bending vibration of a thin plate with small-amplitudes. The plain stress condition is valid, since the thickness h of ABM is small compared with the width or length.
(2) The fluid flow is assumed as incompressible, since $O(\omega^2 L^2/c^2)$ is 10^{-2}–10^{-6}, where the angular frequency ω is $O(10^3)$–$O(10^5)$, the characteristic length L is $O(10^{-3})$, and the sound velocity c is $O(10^3)$.
(3) The effects of gravity and viscosity of surrounding fluid are ignored.

The governing equation for the bending vibration of a plate with isotropic mechanical properties can be described as

$$\rho_m h \frac{\partial^2 w}{\partial t^2} + D\left[\frac{\partial^4 w}{\partial x^4} + 2\frac{\partial^4 w}{\partial x^2 \partial y^2} + \frac{\partial^4 w}{\partial y^4}\right] = p_0 \quad (1)$$

where D, p_0, w, and ρ_m are the bending rigidity, the pressure of acoustic wave, the displacement in z direction, and the density of ABM, respectively. The bending rigidity D is related to Young's modulus E as

$$D = \frac{Eh^3}{12(1-\nu^2)} \tag{2}$$

where ν is the Poisson ratio.

The basic equation for the fluid flow is the Laplace equation of velocity potential ϕ_f as

$$\frac{\partial^2\phi_f}{\partial x^2} + \frac{\partial^2\phi_f}{\partial y^2} + \frac{\partial^2\phi_f}{\partial z^2} = 0 \tag{3}$$

The velocity potential ϕ_f is related to the velocity components (u_x, u_y, u_z) as

$$u_x = \frac{\partial\phi_f}{\partial x}, \quad u_y = \frac{\partial\phi_f}{\partial y}, \quad u_z = \frac{\partial\phi_f}{\partial z} \tag{4}$$

respectively. The subscript f is u or l, where u and l indicate the fluid at the upper and lower sides of ABM, respectively. Furthermore, the velocity potential ϕ_f is related to the pressure as

$$\rho_f\frac{\partial\phi_f}{\partial t} = -p_f \tag{5}$$

where ρ_f is the density of fluid.

The governing equations are solved with the following boundary conditions. The normal velocities at the wall of fluid channel are written as

$$u_z = \frac{\partial\phi_l}{\partial z} = 0 \quad \text{at} \quad z = -L_2 \tag{6}$$

$$u_y = \frac{\partial\phi_l}{\partial y} = 0 \quad \text{at} \quad y = \pm\frac{L_1}{2} \tag{7}$$

where L_1 and L_2 are the width and the depth of fluid channel, respectively. The kinematic boundary condition at $z=0$ is written as

$$\frac{\partial w}{\partial t} = \frac{\partial\phi_f}{\partial z} \quad \text{at} \quad z = 0 \tag{8}$$

The thickness h of ABM is ignored in the analysis of fluid flow, since it is relatively small compared with the depth L_2 of fluid channel. The pressure p_0 is the pressure difference between the upper and lower sides of ABM and can be written as

$$p_0 = -\rho_l\frac{\partial\phi_l}{\partial t} + \rho_u\frac{\partial\phi_u}{\partial t} \quad \text{at} \quad z = 0 \tag{9}$$

Since ρ_l is extremely large compared with ρ_u in the present experiment, Eq. (9) is approximated as

$$p_0 \cong -\rho_l\frac{\partial\phi_l}{\partial t} \quad \text{at} \quad z = 0 \tag{10}$$

To obtain the oscillatory solution at the periodic steady state, following assumptions are made.

(4) A single mode $\eta(x, y)$ is used for the shape function of ABM's bending in y direction. $\eta(x, y)$ is determined based on the analytical solution of a vibrating beam with the first mode, the length of $b(x)$, and the fixed boundary conditions at $y = \pm b(x)/2$ as

$$\eta(x,y) = \begin{cases} c_1\cos\left(\dfrac{\beta}{b(x)}y\right) + c_2\cosh\left(\dfrac{\beta}{b(x)}y\right) & \text{at } -\dfrac{b(x)}{2} \le y \le \dfrac{b(x)}{2} \\ 0 \quad \text{at } -\dfrac{L_1}{2} \le y \le -\dfrac{b(x)}{2} \quad \text{and} \quad \dfrac{b(x)}{2} \le y \le \dfrac{L_1}{2} \end{cases} \tag{11}$$

where c_1, c_2, and β are constants of 0.8827, 0.1173 and 4.730, respectively. These constants are determined to make $\eta(x, y)$ satisfy the fixed boundary conditions at $y = \pm b(x)/2$.

(5) The wave is considered as a slowly varying wave in x direction. That is, the wave number $k(x)$ is slowly varying along x as $b(x)$, where $db(x)/dx \cong 0$ and $dk(x)/dx \cong 0$ are reasonable in the scale of a one wavelength. In this case, the waves can be treated as pseudo plane ones and can be described by the WKB asymptotic solution [10].

Based on these assumptions described above, the displacement $w(x, y, t)$ of ABM can be written as

$$w = W(x)\,\eta(x,y)\,e^{i\int_0^x k(\xi)d\xi}e^{-i\omega t} \tag{12}$$

where i and $W(x)$ are the imaginary number and the envelope function, respectively. $W(x)$ is also treated as a slowly varying function, that is $dW(x)/dx \cong 0$, since the effect of $dW(x)/dx$ on the dispersion relationship is trivial for linear problems [14]. The main purpose of the theoretical analysis is to predict the distribution of the local resonant frequency and to clarify the effect of the surrounding fluid on the resonance. Therefore, to simplify the mathematical development, only the forward wave is included in the analysis. On the other hand, the solution for Eq. (3) which satisfies the boundary conditions of Eqs. (6) and (7) is written as

$$\phi_l = \sum_{j=0}^{\infty} A_j\cosh\left[\zeta_j(z+L_2)\right]\cos\left(\frac{j\pi}{L_1}y\right)e^{i\int_0^x k(\xi)d\xi}e^{-i\omega t} \tag{13}$$

where A_j and ζ_j are the Fourier coefficient for jth mode and $[k^2(x)+(j\pi/L_1)^2]^{1/2}$, respectively. From Eqs. (8), (12) and (13), the following equation is obtained:

$$i\omega W(x)\eta(x,y) = -\sum_{j=0}^{\infty} A_j\zeta_j\sinh(\zeta_j L_2)\cos\left(\frac{j\pi}{L_1}y\right) \tag{14}$$

Using the orthogonality of cosine function, A_j is calculated as

$$A_j = -\frac{i\omega W(x)\int_{-b(x)/2}^{b(x)/2}\eta(x,y)\cos\left(j\pi y/L_1\right)dy}{\zeta_j\sinh\left(\zeta_j L_2\right)\int_{-L_1/2}^{L_1/2}\cos^2\left(j\pi y/L_1\right)dy} \tag{15}$$

Eqs. (10) and (12) are substituted into Eq. (1). Then, multiplying $\eta(x, y)$ to Eq. (1), and integrating from $-b(x)/2$ to $b(x)/2$ with respect to y, the following eikonal equation is obtained:

$$\begin{aligned} f(x,\omega) &= D\left[k^4(x)\int_{-b(x)/2}^{b(x)/2}\eta^2(x,y)\,dy - 2k^2(x)\right. \\ &\times\left.\int_{-b(x)/2}^{b(x)/2}\eta(x,y)\,\partial^2\eta(x,y)/\partial y^2 dy + \left[\beta/b(x)\right]^4\int_{-b(x)/2}^{b(x)/2}\eta^2(x,y)\,dy\right] \\ &-\omega^2\left[\rho_m h\int_{-b(x)/2}^{b(x)/2}\eta^2(x,y)\,dy + \rho_l\sum_{j=0}^{\infty}\frac{\left[\int_{-b(x)/2}^{b(x)/2}\eta(x,y)\cos\left(j\pi y/L_1\right)dy\right]^2}{\zeta_j\tanh\left(\zeta_j L_2\right)\int_{-L_1/2}^{L_1/2}\cos^2\left(j\pi y/L_1\right)dy}\right] \end{aligned} \tag{16}$$

Eq. (16) describes the dispersion relationship between $k(x)$ and ω at various x. The effect of surrounding fluid is found in the last term of Eq. (16). Since this term contributes to increase the effective mass for the vibration, the resonant frequency may be decreased by the surrounding fluid. From the average variation principle [14], it is known that the eikonal equation has the relationship with $W(x)$ as

$$W(x) = \frac{c}{\left(\frac{\partial f}{\partial k}\right)^{1/2}} \tag{17}$$

Table 1
Parameters for prediction.

Parameter	Symbol	Value
Width of ABM (m)	$b(x)$	$b(x)=0.002+0.002x/L_3$
Young's modulus of PVDF (Pa)	E	3×10^{9}[a]
Width of fluid channel (m)	L_1	0.017
Depth of fluid channel (m)	L_2	0.004
Length of ABM (m)	L_3	0.03
Poisson ratio of PVDF	ν	0.29[a]
Density of PVDF (kg/m^3)	ρ_m	1780 [15]
Density of silicone oil (kg/m^3)	ρ_s	873[b]
Density of air (kg/m^3)	ρ_a	1.2 [16]

[a] From technical report by KUREHA.
[b] From technical report by Shin-Etsu Chemical.

where c is a constant. Eq. (17) is the transport equation which describes the qualitative distribution of $W(x)$.

The parameters for the prediction are listed in Table 1. If the angular frequency ω is given as that of externally applied acoustic wave, only the wave number $k(x)$ is a variable to be solved in Eq. (16), where Eq. (16) is reduced to $f(k(x))=0$. At various ω, Eq. (16) is solved numerically by the Newton method. The iteration procedure is repeated until the residual becomes less than a specified tolerance of 10^{-6}. The term including summation is treated from $j=0$ to 30, which is adequate for the tolerance. The calculation is conducted for the two cases of filling the fluid channel with the air and of that with the liquid. The frequency is changed in the ranges of 3.5–14.0 kHz in the air environment and 0.7–3.6 kHz in the liquid environment, respectively. At those frequencies, Eq. (16) gives solutions and $W(x)$ has a peak on ABM.

Fig. 3 shows $W(x)$ which describes the qualitative amplitude distribution defined by Eq. (17). $W(x)$ in the air environment of Fig. 3(a) shows a clear peak at each frequency, where the peak indicates the resonance at the local place. Comparing $W(x)$ at different frequencies, it is found that the peak position shifts to smaller x as the frequency increases. It is also found that the peak value of $W(x)$ decreases as the frequency increases. Fig. 3(b) shows the $W(x)$ in the liquid environment. As same with the result in the air environment, the peak position shifts to smaller x as the frequency increases. However, compared with the results in the air environment, $W(x)$ in the liquid environment shows peaks at smaller frequencies. By comparing the results at 3.5 kHz in Fig. 3(a) and (b), the effect of the surrounding fluid on $W(x)$ can be discussed in detail. Although ABM is vibrated at the same frequency, it is found that the peak position in the liquid environment is shifted to smaller x and the form of $W(x)$ is moderated compared with those in the air environment. These results indicate that the stronger fluid-structure interaction due to the higher density decreases the resonant frequency and relaxes the resonance. Based on Eq. (16), the mechanism of decreasing the resonant frequency in the liquid environment is that the effective mass for the vibration is increased due to the much higher density of the liquid compared with that of the air. The reason for the moderated resonance is discussed later.

Fig. 4(a) shows the distributions of $k(x)$ in the air environment at 3.5, 6.0, 9.0, and 12.0 kHz. In Fig. 4(a), it is found that $k(x)$ in the air environment increases with x. There is a certain position of x_{inc} where $k(x)$ rapidly increases. x_{inc} is mathematically defined as the position where $k(x)$ gives the largest gradient. At larger x than x_{inc}, $O(k(x))$ is 10^2–10^3 m^{-1} and the wavelength is 63–6.3 mm. At smaller x than x_{inc}, $k(x)$ is very small which corresponds to the extremely long wavelength. Comparing the results at different frequencies, it is found that x_{inc} becomes smaller at the higher frequency. It is also found that x_{inc} is close to the peak position of $W(x)$ in Fig. 3(a). Since the result is obtained by the analysis based on the WKB solution, the wavelength should be short enough to treat $b(x)$ as a slowly varying function. Furthermore, $k(x)$ should be gradually changed by x. Thus, the precision of result should be relatively bad around x_{inc} and at smaller x than x_{inc}. Fig. 4(b) shows the $k(x)$ distributions in the liquid environment at 1.0, 2.0, 3.0, and 3.5 kHz. $k(x)$ in the liquid environment gradually increases with x compared with that in the air environment. Although the resonant frequencies are different between in the air and in the liquid envi-

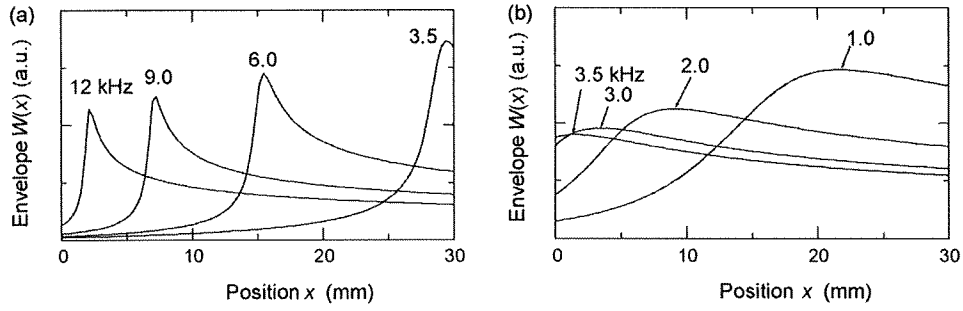

Fig. 3. Theoretical results of envelope function $W(x)$ in (a) air and in (b) liquid environments for various frequencies.

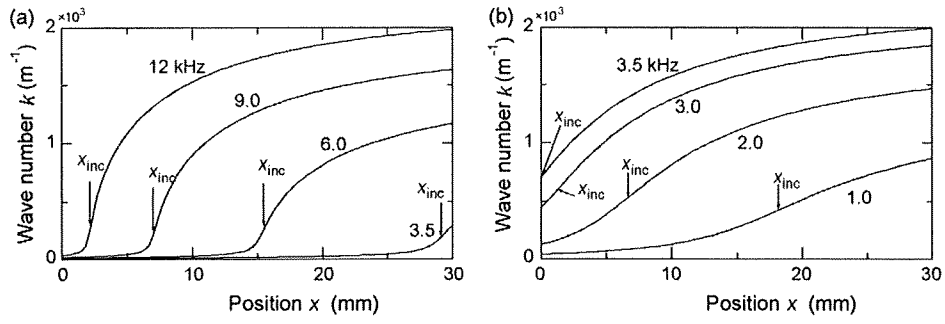

Fig. 4. Theoretical results of wave number $k(x)$ in (a) air and in (b) liquid environments for various frequencies.

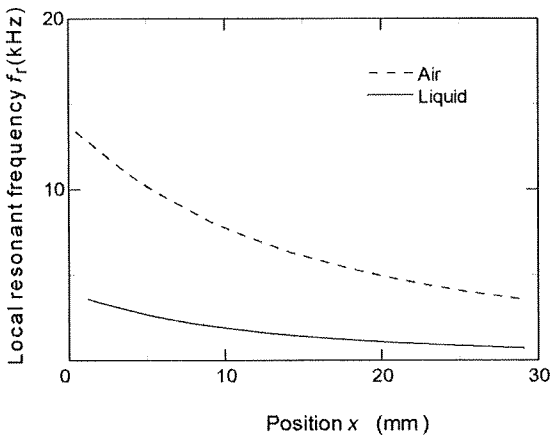

Fig. 5. Theoretical results of local resonant frequencies in air and in liquid environments.

ronments, the orders of $k(x)$ around x_{inc} and at larger x than x_{inc} are similar to the results in the air environment. From this result, it can be said that the resonance is governed by the wavelength which is strongly related to the geometry of ABM. x_{inc} is closely connected with the peak position of $W(x)$ shown in Fig. 3(b). Furthermore, the reason for the moderated resonance in the liquid environment can be explained by comparing Fig. 4(a) and (b). Since $k(x)$ in the air environment rapidly changes around the resonance place as shown in Fig. 4(a), the evolution of $W(x)$ also does. It is owing to the fact that the resonance condition is governed by the wavelength. On the contrary, since $k(x)$ in the liquid environment gradually changes around the resonance place as shown in Fig. 4(b), the peak of $W(x)$ becomes to be moderated.

Fig. 5 shows the relationship between the resonant frequency f_r and x. Both f_r in the air and in the liquid environments decrease as x increases and f_r in the liquid environment is lower than that in the air environment due to the increase of effective mass. Although the auditory frequency is widely ranged from 20×10^{-3} to 20 kHz, the device can cover only the part of it. It works at the frequencies over the ranges of 3.5–14 kHz in the air environment and 0.7–3.6 kHz in the liquid environment, respectively. For the clinical application, the device should be optimized to realize the frequency selectivity in the required frequency range for a daily conversation. Furthermore, distribution of f_r should be fitted to that in the biological system from the viewpoint of natural hearing. To solve these problems, the geometrical optimizations of ABM can be effectively carried out in our future work based on the theoretical analysis developed here.

The theoretical analysis is carried out based on the experimental condition, where only the bottom side of ABM faces to the liquid. In case of ABM facing to the liquid at both sides, the difference is found in the last term of Eq. (16) which includes the effect of surrounding fluid. In case of the same fluid channel is placed on the upper side of ABM and is filled with the same liquid, the last term is double of that in Eq. (16). Consequently, the larger effect of surrounding fluid is induced, that is, the further decrease of resonant frequency is found due to the increase of effective mass for the vibration, where the figure is omitted.

Furthermore, the theoretical analysis is carried out based on the assumption of the small amplitude. The basic equations are solved by WKB treatment which cannot quantitatively predict the vibrating amplitude. Therefore, it is difficult to precisely estimate the piezoelectric output which is determined by the strain in the membrane. The investigation on the piezoelectric output can be made by the numerical analysis based on the finite element method, which is our future research.

3. Results and discussion

3.1. Performance test in air environment

The basic vibrating characteristics of ABM in the air environment are investigated as a preliminary experiment. This experiment is conducted without filling the fluid channel with the silicone oil. The amplitude distributions of vibration are measured by applying acoustic waves of 75 dBSPL. The frequency is controlled over the range of 1.0–20.0 kHz, which covers the part of human's audible frequency. The amplitude of vibration becomes relatively small at the frequencies both lower than 3.0 kHz and higher than 18.0 kHz. It may be owing to that ABM is designed to have LRF for the first mode over the range of 3.5–14.0 kHz in the air environment. Fig. 6(a)–(d) show the amplitude distribution at f = 4.0, 6.0, 9.0, and 12.0 kHz, respectively. The amplitude distribution clearly shows dependence on the frequency. The place with maximum amplitude, where ABM is locally resonating, shifts to the smaller x as the frequency increases. This relationship between the position of resonating place and the frequency successfully has similarities with that of biological basilar membranes. Furthermore, in Fig. 6(c) and (d), it is found that there are several extrema indicated by arrows at the larger x than that of resonating place. These may be induced by the standing wave due to the traveling waves to positive and negative directions of x. The reason why the standing wave is not observed at the smaller x than that of resonating place is that the wavelength is relatively long at those positions. This is confirmed by the theoretical result of relatively small $k(x)$ as shown in Fig. 4(a). In the biological cochlea, the acoustic wave travels from the basal to the apex. However, in our experiment, it is applied to the entire ABM from the air. As a result, the relatively large effects of the standing waves are induced in our experiment due to the small damping effects from the surrounding fluid.

Fig. 7(a)–(c) show the frequency dependences of vibration and the piezoelectric output at Ch. 6, Ch. 12 and Ch. 18, respectively. The amplitudes of vibration and the piezoelectric output are plotted by a solid line and by a broken line, respectively. It seems that each electrode has a specific frequency where the electrode gives

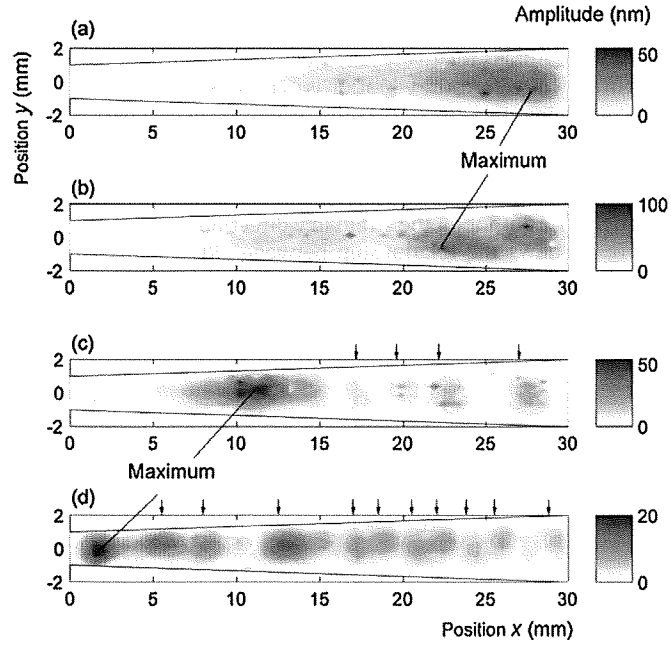

Fig. 6. Experimental results of contour maps of vibration amplitude at (a) f = 4.0 kHz, (b) 6.0 kHz, (c) 9.0 kHz, and (d) 12.0 kHz in air.